Year-to-Year Reoutcropping of Eighteen Degree Water in an Eddy-Resolving Ocean Simulation

YOUNG-OH KWON

Woods Hole Oceanographic Institution, Woods Hole, Massachusetts

JONG-JIN PARK

Department of Oceanography, Kyungpook National University, Daegu, South Korea

STEFAN F. GARY

Scottish Association for Marine Sciences, Oban, United Kingdom

M. SUSAN LOZIER

Division of Earth and Ocean Sciences, Duke University, Durham, North Carolina

ABSTRACT

Winter outcropping of the Eighteen Degree Water (EDW) and its subsequent dispersion are studied using a $1/12°$ eddy-resolving simulation of the Family of Linked Atlantic Modeling Experiments (FLAME). Outcropped EDW columns in the model simulations are detected in each winter from 1990 to 1999, and particles are deployed in the center of each outcropped EDW column. Subsequently, the trajectories of these particles are calculated for the following 5 yr. The particles slowly spread away from the outcropping region into the nonoutcropping/subducted EDW region south of ~30°N and eventually to the non-EDW region in the greater subtropical gyre. Approximately 30% of the particles are found in non-EDW waters 1 yr after deployment; after 5 yr, only 25% of the particles are found within EDW. The reoutcropping time is defined as the number of years between when a particle is originally deployed in an outcropping EDW column and when that particle is next found in an outcropping EDW column. Of the particles, 66% are found to reoutcrop as EDW in 1 yr, and less than 5% of the particles outcrop in each of the subsequent 4 yr. While the individual trajectories exhibit significant eddy-like motions, the time scale of reoutcropping is primarily set by the mean circulation. The dominance of reoutcropping in 1 yr suggests that EDW outcropping contributes considerably to the persistence of surface temperature anomalies from one winter to the next, that is, the reemergence of winter sea surface temperature anomalies.

1. Introduction

Mode water is one of the most noticeable and ubiquitous features in the upper ocean, marked and defined by a thick layer of homogeneous properties and found adjacent to strong ocean fronts in many parts of the global ocean (Hanawa and Talley 2001; Speer and Forget 2013). The North Atlantic Subtropical Mode Water, also often called the Eighteen Degree Water (EDW), is the most extensively studied among them, along with the North Pacific Subtropical Mode Water. It was first observed during the *Challenger* expedition in 1873 (Wyville-Thompson 1877), and Worthington (1959) named it after its homogenous temperature of ~18°C.

The EDW is a thick, homogeneous, low potential vorticity (PV) layer found in the upper 500 m over a vast area of the subtropical North Atlantic to the west of the Mid-Atlantic Ridge between the Gulf Stream and ~20°N. It appears as a mode around 18°C and 36.5 psu from a volumetric census (Worthington 1976; Joyce 2012). It is replenished during winter when outcropped

Corresponding author address: Young-Oh Kwon, Physical Oceanography Department, Woods Hole Oceanographic Institution, MS 21, Woods Hole, MA, 02543.
E-mail: yokwon@whoi.edu

to the surface as a result of intense surface buoyancy loss near the Gulf Stream (Worthington 1972; Talley and Raymer 1982; Maze et al. 2009; Joyce et al. 2013). Once the surface buoyancy flux changes sign in early spring, the upper ocean restratifies and EDW is isolated from direct contact with the atmosphere for the rest of the year. While EDW outcrops during winter in the northern half of the region, it is only found below the thermocline in the southern half of the region (Kwon 2003; Forget et al. 2011; Maze and Marshall 2011; Kelly and Dong 2013).

Because it is formed in the winter, EDW is at maximum volume in that season. A rapid decrease in volume occurs during the restratification in spring and summer, and then there is a continued slower dissipation from late summer to the end of fall (Kwon and Riser 2004; Forget et al. 2011; Davis et al. 2013). The difference between the late winter maximum and the late fall minimum volumes, which is the annual destruction rate of EDW, ranges from ~30% to 80% of peak winter volume depending on the EDW definition, its spatial extent, and the temporal resolution of the data used for this measure (Kwon and Riser 2004; Forget et al. 2011; Joyce 2012). Based on an ocean state estimate for 2004–06, Forget et al. (2011) attributed the significant annual destruction primarily to the surface buoyancy gain during the warming season and secondarily to internal mixing.

The Walin (1982) water mass framework provides a way to quantify the transformation and formation rates of a water mass bounded by isopycnal or isothermal surfaces (Speer and Tziperman 1992; Marshall et al. 1999). This framework has often been applied to the EDW, especially to quantify its annual formation (and destruction) because of the surface air–sea buoyancy fluxes. For example, Maze et al. (2009) reported that the annual formation rate of the EDW (bounded by the 17° and 19°C SST isotherms) is 3–5 Sverdrups (Sv; $1\,\mathrm{Sv} \equiv 10^6\,\mathrm{m}^3\,\mathrm{s}^{-1}$) with a peak in February. In addition to the formation and transformation rates integrated across the basin, Maze et al. (2009) examined the spatial distribution of the formation and transformation rates and found that the EDW forms primarily to the west of 45°W, between the Gulf Stream and 30°N.

As the EDW is a pool of low PV water, the annual cycle of EDW can also be studied in terms of its PV budget, similar to the Walin diathermal or diapycnal volume flux approach, but in a more dynamical context. Maze and Marshall (2011) used the flux form of a PV conservation equation to diagnose where and when PV is extracted from the EDW. They found that the low PV of the EDW is primarily sustained by the vertical PV flux at the surface driven by the air–sea buoyancy fluxes,

with the surface mechanical flux playing a secondary role (also see Maze et al. 2013; Olsina et al. 2013). In addition, Maze and Marshall (2011) approximated the circulation path of this low PV water using the annual-mean Bernoulli function (i.e., the PV flux streamlines) on 26.4 σ_θ (also see Deremble et al. 2014). Deremble and Dewar (2013), however, applied a PV budget to a control volume defining EDW in an eddy-resolving ocean model simulation to find that the lateral PV flux across the interior boundary outweighs the surface PV flux. They showed a balance between the lateral mean flux (which acts to export PV from the low PV pool) and the lateral eddy flux (which acts to import higher PV).

In addition to the annual cycle, the EDW exhibits pronounced interannual variability (Talley and Raymer 1982; Alfultis and Cornillon 2001; Kwon and Riser 2004; Dong et al. 2007). Based on the 40-yr time series of EDW volume and temperature constructed from historical temperature profiles for 1961–2000, Kwon and Riser (2004) suggested that the interannual variability of the EDW volume has ~50% larger variance than that of the annual cycle. They also showed that the temperature and volume of the EDW are inversely correlated ($r = -0.8$) on interannual time scales, which is consistent with the fact that the EDW is produced via intense surface heat loss. As the EDW covers a vast area of the subtropical North Atlantic, the upper-ocean heat content and EDW volume are also anticorrelated, and hence the EDW acts as a deficit heat reservoir (Kwon 2003; Dong et al. 2007). Furthermore, since the winter surface heat loss and resulting EDW formation are modulated by the North Atlantic Oscillation (NAO; Cayan 1992; Talley 1996; Dickson et al. 1996), the EDW integrates the NAO surface forcing over 3–5 yr, which is the turnover time scale of EDW (Kwon and Riser 2004). If the ocean memory retained by EDW influences air–sea interaction in subsequent winters, it could result in some persistence of climate variability in the region from year to year. In addition to the anomalous heat, the EDW also acts as an interannual reservoir for anomalous nutrients and CO_2 in the upper ocean (Bates et al. 2002; Palter et al. 2005).

A crucial step toward a better understanding of whether and how anomalous heat, nutrients, and CO_2 stored in the EDW from the past 3–5 winters influence the EDW's interaction with the atmosphere and surface mixed layer in subsequent winters is an improved understanding of EDW pathways following its formation (when the anomalous properties are imprinted). Gary et al. (2014) used Lagrangian trajectories of particles launched within the EDW in an eddy-resolving ocean general circulation model hindcast simulation to study their fate as they moved away from the formation

region. The spreading of particles followed the large-scale circulation, consistent with the large-scale PV field with an eddy-driven mean flow in the southern portion of the EDW domain. The particles frequently exited and reentered the EDW while spreading, with an average residence time of ~10 months. The particles lost the EDW properties (i.e., exited EDW) primarily because of an increase in stratification (equivalently PV). The temperature, stratification, density, and PV anomalies along the trajectories had an average integral time scale of ~3 months, indicating strong mixing. While these time scales are much shorter than the ~3–4-yr turnover time for EDW estimated from previous studies (Jenkins 1982; Kwon and Riser 2004; Maze and Marshall 2011), Gary et al. (2014) showed that the turnover time in the Eulerian frame based on the annual cycle of EDW volume (~3 yr) is consistent with the turnover time calculated from the particle inventory.

While the Walin-type water mass formation rate and PV budget have been shown to be useful for understanding the overall volume flux and PV budget of the EDW, especially related to formation, the Lagrangian approach of Gary et al. (2014) highlighted the pathways and fate of the EDW parcels following formation. Along their Lagrangian pathways the EDW parcels are subject to the same PV and diabatic fluxes considered in the Eulerian volume and PV flux calculations, for example, the air–sea fluxes, mixed layer entrainment/restratification, and interior eddy mixing, all of which change the properties of the parcels along their pathways.

In this paper, we examine a subset of the particle trajectories from Gary et al. (2014). Our goal is to understand how and when EDW parcels reoutcrop and the implications of that outcropping on year-to-year persistence of thermal anomalies in the upper ocean. Section 2 describes the model simulation and experimental design, and the model simulation is assessed against available data in section 3. The main results are presented in section 4. Last, section 5 contains the summary and discussion.

2. Model simulation and experiment design

a. Brief description of the FLAME simulation

A hindcast simulation for 1990–2004 using an eddy-resolving ocean general circulation model at $1/12°$ resolution is used in this study. The model is the highest-resolution member of the Family of Linked Atlantic Modeling Experiments (FLAME) and has been used extensively to examine various aspects of the North Atlantic circulation (e.g., Böning et al. 2006; Biastoch et al. 2008;

Gary et al. 2011, 2014; Burkholder and Lozier 2011). This primitive equation, z-coordinate, regional model is based on the Modular Ocean Model (MOM2.1) (Pacanowski 1996) with isopycnal mixing and biharmonic friction and the addition of a bottom boundary layer (Beckmann and Döscher 1997). The parameterization of convection is realized in the model using the scheme of S. Rahmstorf (1993, unpublished manuscript), which homogenizes water mass properties vertically among unstably stratified grids. The model also uses the mixed layer parameterization of Kraus and Turner (1967), and the vertical mixing is parameterized after Cummins et al. (1990). The model domain spans the Atlantic Ocean from 18°S to 70°N. Vertically, the model has 45 levels with 10-m spacing near the surface and maximum of 250 m spacing below 2000 m. [Refer to Czeschel (2004) for more detail on the model configuration.]

The model was spun up for 10 yr with initial conditions from January climatological temperature and salinity anomalies of Levitus et al. (1994) and Levitus and Boyer (1994) superimposed on the annual means of Boyer and Levitus (1997) under ECMWF climatological forcing. Then the interannual anomalies from the NCEP–NCAR reanalysis (Kalnay et al. 1996) were added to the climatological forcing to drive the hindcast simulation for 1990–2004. The 3-daily (i.e., every third day) snapshots and monthly averages of horizontal velocity, temperature, and salinity, saved during the hindcast simulation, are used for this study.

b. EDW definitions

The definition of EDW used in this study is based on that from Kwon and Riser (2004) but slightly modified. Their original definition defines a portion of the profile as the EDW layer when the following two primary criteria are satisfied simultaneously: 1) temperature should be between 17° and 19°C, and 2) the vertical temperature gradient should be smaller than $0.006°C m^{-1}$. This definition is based only on the potential temperature profile to maximize the use of temperature-only profiles in the historical archives. The vertical temperature gradient criterion corresponds approximately to a potential density gradient smaller than $0.0015 kg m^{-4}$ and a PV smaller than $1 × 10^{-10} m^{-1} s^{-1}$, both of which have been used in previous EDW studies (e.g., Talley and Raymer 1982; Billheimer and Talley 2013).

For the observational data used in this study, the original Kwon and Riser (2004) definition is applied. However, based on the model data comparison presented in the following section 3, a slightly relaxed EDW definition is applied to the FLAME profiles. The EDW definition modified for the FLAME profiles is 1) temperature should be between 17° and 20°C, and 2) the

vertical temperature gradient should be smaller than $0.010°C\,m^{-1}$. The sensitivity of the results to the definition is tested by changing the temperature range to 17°–19°C and/or the temperature gradient criterion to $0.006°C\,m^{-1}$. Overall, the results presented in the following sections are robust regardless of which of these definitions is chosen.

A couple of secondary criteria are applied to ensure appropriate detection of EDW. First, the EDW layer should be thicker than 50 m to avoid relatively shallow mixed layers that are not part of the main body of EDW. Second, because temperature profiles can contain multiple discontinuous EDW layers that satisfy the above criteria, we set a condition that the thickest layer is the EDW layer. However, to allow for the possibility of small-scale overturnings in the observed profiles, we permit discontinuities smaller than 10 m within the EDW layer (consistent with the maximum vertical resolution of 10 m in the FLAME profiles) and consider the EDW layers above and below those small discontinuities as one EDW layer.

These criteria provide the upper and lower bounds for the EDW layer in each temperature profile. Outcropping EDW columns are defined as those EDW columns with their upper bound at the sea surface. This definition is applied to the FLAME model output as well as to the observations.

c. Particle deployment strategy and trajectory calculation

Using the FLAME 3-day temperature profiles, once an outcropped EDW layer is identified at a grid point, a particle is deployed at the vertical midpoint of that layer, and then the trajectory of the particle is calculated offline for the next 5 yr using the three-dimensional, 3-day velocity field from FLAME. While the horizontal velocities are part of the model output, the vertical velocity is calculated from the divergence of horizontal velocities at each grid box for each 3-day time step. [Note that Gary et al. (2011) showed that offline trajectory calculations based on 3-day snapshots of the three-dimensional velocity are practically equivalent to those using daily snapshots.]

To find outcropped EDW, the FLAME temperature profiles at every twelfth grid node (thus approximately 1° × 1° resolution) rather than every grid node are searched. A similar sampling strategy is applied temporally: the search is conducted with 12-day intervals between 15 February and 15 April for each winter between 1990 and 1999. In addition, the search is limited to the west of 35°W to avoid sampling the Madeira Mode Water, which is a distinct water mass (Siedler et al. 1987). Note that the particles used in this study are a subset of those used by Gary et al. (2014). More specifically, Gary et al. (2014) deployed particles throughout the outcropped EDW column at 20-m interval, while only one particle for each outcropped EDW column deployed at the center is used here. See Gary et al. (2014) for additional details regarding the handling of particles. A total of 49 753 particles were deployed in this manner over the 10 winters from 1990 to 1999.

In addition, upper and lower bounds of the EDW layer, if present, are calculated at each particle time and position to determine whether or not the particle is in the EDW layer at that given time and location. A particular focus is given to the particles found in the outcropping EDW layers. When a particle is found in an outcropping EDW column in subsequent winters, it is called "reoutcropping as EDW," even though it is EDW, not the particle itself, that is actually (re)outcropping.

3. Model data comparison

a. EDW distribution

Three types of observational data are used to validate the FLAME simulation for the aspects most relevant to the focus of this paper. Figure 1 compares the temperature, salinity, and vertical temperature gradients along a meridional section at ~52°W, across the middle of the region occupied by EDW. The observational fields are from the Word Ocean Circulation Experiment (WOCE) A20 CTD section occupied from 17 July to 10 August 1997 (Joyce et al. 1999). The FLAME temperature section on 28 July 1997 compares reasonably well with the observed field in the vicinity of the EDW layer. The thickness of the layer between 17° and 19°C is realistic. However, the stratification is slightly higher at 17°–19°C, while slightly weaker in the simulation in the range of 19°–21°C. Overall, vertical temperature gradients in FLAME show a weaker thermostad (as indicated by the relatively small area colored with the darkest blue) compared to observations, which may be attributable to insufficient vertical resolution around the EDW layer and/or overly diffusive model dynamics in this region. The thickness of the homogeneous layer in the observed salinity section is also reasonably reproduced in the model, but the salinity is fresher in FLAME by ~0.1 psu. As described in the previous subsection, these comparisons indicate a need for slightly relaxed EDW criteria for FLAME. With this relaxed definition, we note that the EDW layer (with boundaries indicated by white contours) is slightly thicker in FLAME than in the observations.

For further validation of FLAME's ability to reproduce EDW, the spatial distribution of EDW thickness
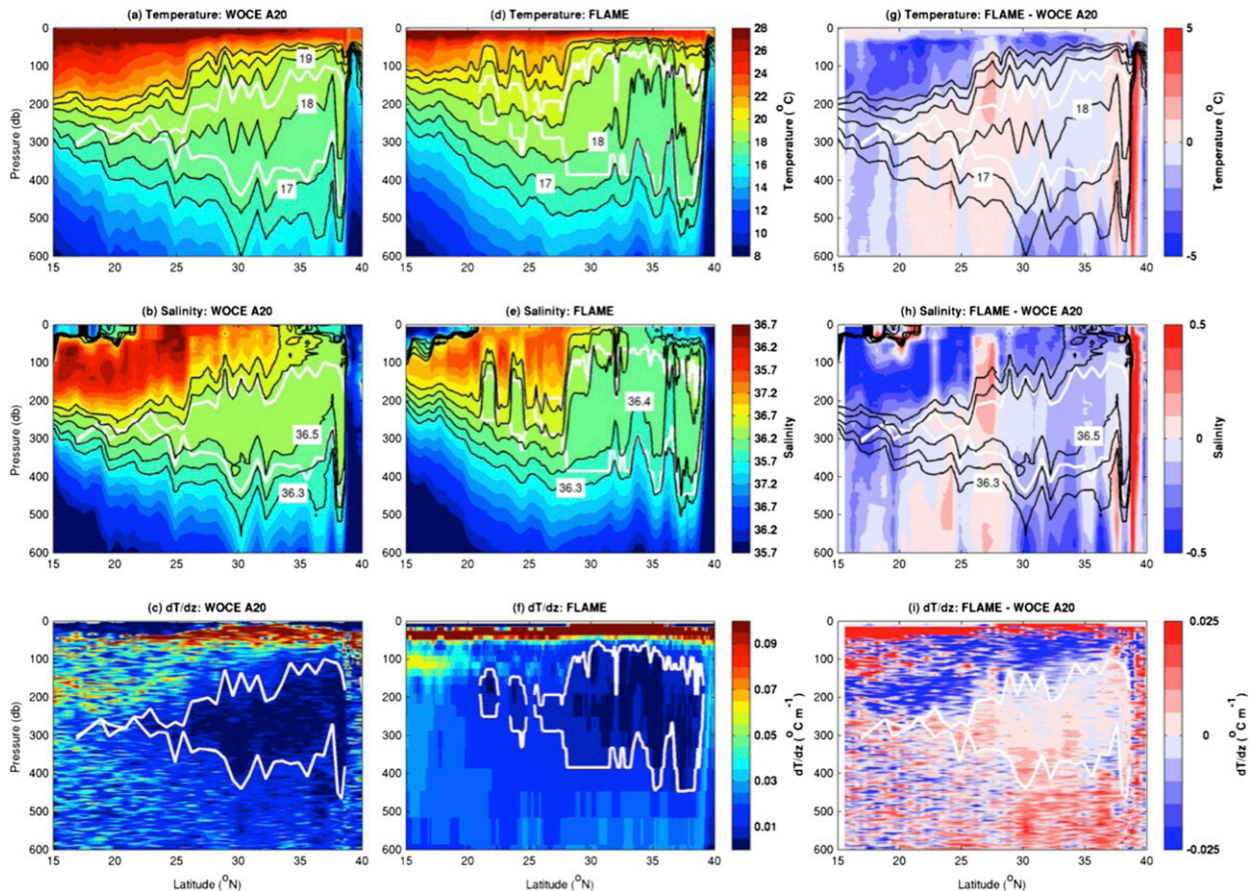
FIG. 1. (a)–(c) The WOCE A20 section along ~52°W (17 Jul–10 Aug 1997), (d)–(f) the corresponding section from a FLAME simulation on 28 Jul 1997, and (g)–(i) the difference between the two (i.e., FLAME minus WOCE). The contour intervals for (top) potential temperature, (middle) salinity, and (bottom) vertical temperature gradient are 1°C, 0.1, and 0.005°C m^{-1}, respectively, and the black contours indicate 16°–21°C in (a),(d), and (g) and 36.3–36.7 in (b),(e), and (h). The white contours denote the upper and lower boundaries of EDW as defined in the text. For the difference plots in (g)–(i), the black and white contours are from the WOCE A20 sections.

and the extent of the EDW outcropping region from FLAME are compared to those computed from profiling float observations. Profiling float data during 1998–2008 from three different observational programs, that is, the WOCE/Atlantic Climate and Circulation Experiment (ACCE) (1998–2004; Kwon and Riser 2005), Argo (2000–11; www.argo.ucsd.edu), and CLIVAR Mode Water Dynamics Experiment (CLIMODE) (2006–08; Marshall et al. 2009), are used; a total of ~5700 temperature profiles are available for the primary outcropping season (February–April). A comparison (Fig. 2) shows that both the observed and modeled EDW are thicker in the northern half of the region, north of ~30°N, and become rapidly thinner equatorward. Importantly, the outcropping areas are comparable between FLAME and the observations. Consistent with Fig. 1, EDW in FLAME is thicker by ~100 m. Also, the modeled and observed EDW differ in their patchiness of the thickest EDW; the observed patchiness is not apparent in

FLAME, perhaps partly a result of the uneven sampling/distribution of EDW and eddy fields in the observations and the vast difference in the number of data points between the two (see also Gary et al. 2014, their Fig. 3).

b. EDW trajectories

Continuing with the model data comparison, trajectories of the 40 acoustically tracked, quasi-Lagrangian bobber floats from the CLIMODE program, tracked for ~2 yr between 2006 and 2009, are compared with randomly sampled FLAME trajectories (Fig. 3). The CLIMODE bobber floats were designed to actively follow the 18.5°C isotherm and make a temperature profile between 17° and 20°C every 3 days (Fratantoni et al. 2013). In addition to the 3-day bobbing, the float positions were acoustically tracked with daily resolution, and the bobbers dived to 1000 m before surfacing to transmit the data via Argos satellites every 30 days.
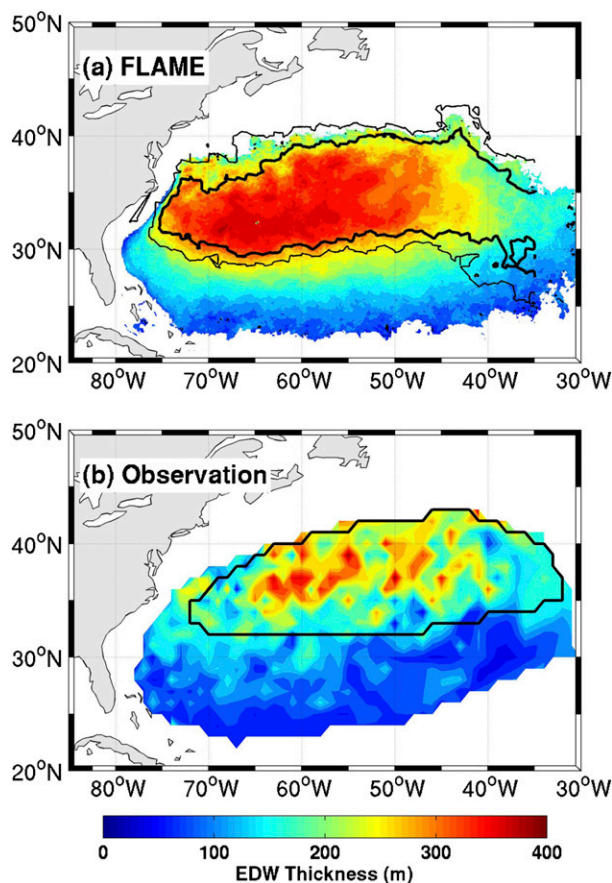
FIG. 2. Spatial distribution of climatological winter (February–April) mean EDW thickness (color) and outcropping region (black contours) from (a) FLAME (1990–2004) and (b) profiling float observations (1998–2008). For FLAME, EDW thickness is calculated at each grid point from the monthly-mean temperatures calculated from the 3-day output. Only grid points where EDW is found in at least 10% of all winter months are included. The profiling float observations are from Argo, WOCE/ACCE, and CLIMODE programs. Temperature from the profiling floats are averaged within $1° \times 1°$ bins and objectively mapped for each month and year as in Kwon and Riser (2004). The EDW thickness is then determined from the mapped temperature profiles as described in Kwon and Riser (2004). The thick black contour for FLAME, determined from the 3-day output, shows where outcropped EDW is found 30% of the time during the three winter months for 10 yr (1990–99). The thin contour corresponds to 10% occurrence. The outcropping region for the observations encompasses the positions of all profiles with outcropped EDW.

While this dataset provides unprecedented quasi-Lagrangian trajectories of EDW, it provides only 43 observations of EDW outcropping with subsequent trajectories of 1 yr or longer that can be visually compared with 43 randomly selected FLAME trajectories in Fig. 3. Each FLAME particle is randomly selected among 40–60 particles initially positioned in outcropping EDW within 1° longitude, 1° latitude, and

1 month (regardless of the year) from each corresponding bobber EDW outcropping. This qualitative comparison suggests reasonable circulation paths of EDW particles following the winter outcropping. However, there is one important difference to keep in mind between the two trajectories. The FLAME particles are advected by the three-dimensional velocity (while the properties are changed by diabatic fluxes along the trajectories). On the other hand, the bobber trajectories are additionally influenced by diathermal fluxes, as they are designed to actively remain within the 17°–20°C layer.

c. EDW outcropping

As described in the previous section, the statistics of the particles at the time of deployment reflect the properties of outcropped EDW in FLAME, which compares reasonably well with the observed properties of outcropped EDW derived from profiling floats, that is, from a combination of the Argo, CLIMODE, and WOCE/ACCE floats, as further described below (Fig. 4). FLAME EDW outcroppings, found mostly between 40° and 65°W, compare favorably with observations, though the particles' distribution extends farther west (Fig. 4a) because of the inclusion of 19°–20°C in the FLAME EDW definition (not shown). Also, the meridional distribution for the particles is biased to the south by ~3° of latitude, peaking around 33°–36°N instead of 35°–39°N as in the observations (Fig. 4b). This southward bias is also evident in Fig. 2. The discrepancy in the southern limit of the outcropping probably results from the more permissive EDW definition for the FLAME profiles (especially with the vertical temperature gradient), while the shift in the northern limit may be related to the slightly excessive Gulf Stream eddy kinetic energy in FLAME, especially to the west of ~60°W (Burkholder and Lozier 2011), which would inhibit the development of a weakly stratified thick EDW layer near the Gulf Stream. The outcropped EDW is thicker in FLAME (with mean and standard deviation being 307 ± 106 m) compared to the observations (284 ± 95 m) (Fig. 4d). Since the particles are deployed near the middle of outcropped EDW columns, the depth of particle deployment is mostly distributed between 160 and 240 m (Fig. 4c).

The timing of particle deployment is similar to the observed outcropping window, except for the fact that the particles are deployed beginning 15 February (Fig. 4e). The number of outcrops in the model, which is a close proxy for the total outcropping area, varies interannually within ±18% of the mean. This interannual variability is much smaller than that from the observations
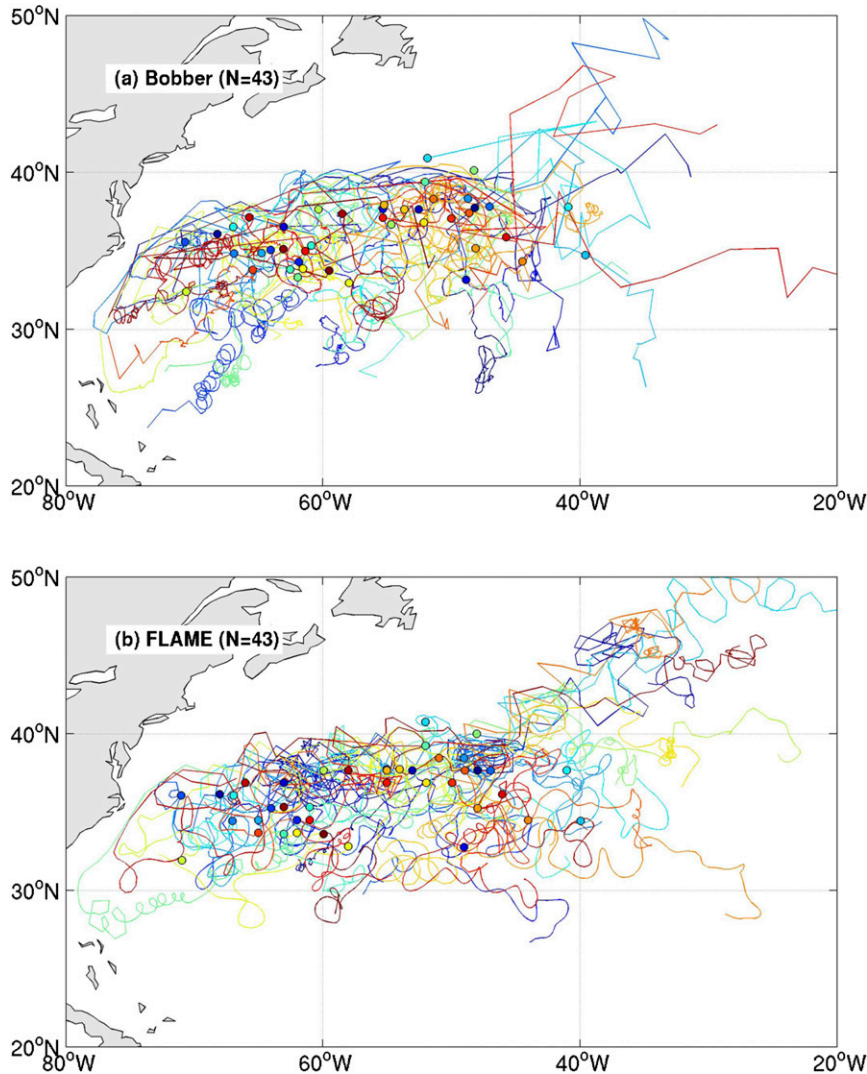
FIG. 3. The 1-yr Lagrangian trajectories starting from each EDW outcropping based on (a) observations using the quasi-Lagrangian bobber floats deployed during the CLIMODE field campaign (November 2005–November 2007) and (b) randomly selected FLAME particle trajectories. Initial positions are indicated with the filled circles with the same color as the corresponding trajectory. Each FLAME particle is selected to match each bobber observation. The match is based on the initial time and location when the EDW outcropped, so that the corresponding bobber and particle are initially within 1 month (regardless of the year) and 1° latitude and 1° longitude. About 40–60 particles satisfy this match criterion for each observation; one of these is randomly picked for this plot.

(Fig. 4f), although the year-to-year difference in the observation more than likely reflects sampling inhomogeneity (cf. Forget et al. 2011).

The mode in the temperature histogram is near 18.25°C for both particles and observations, while particles exhibit an additional tail at 19°–20°C, as expected (Fig. 4g). On the other hand, salinity exhibits a fresh bias in FLAME by ~0.1 psu, with the mode in FLAME around 36.45 psu, consistent with the meridional section in summer (Fig. 1).

4. Results

a. Dispersion of the EDW following outcropping

The particles deployed within each outcropped EDW column disperse for the next 5 yr, as illustrated in Fig. 5 for particles launched in the 1996 winter. Note that the overall characteristics apply to the other winter cases. As the particles disperse from their initial locations, they slowly fill the subtropical gyre to the south of the Gulf Stream–North Atlantic Current. Though many particles
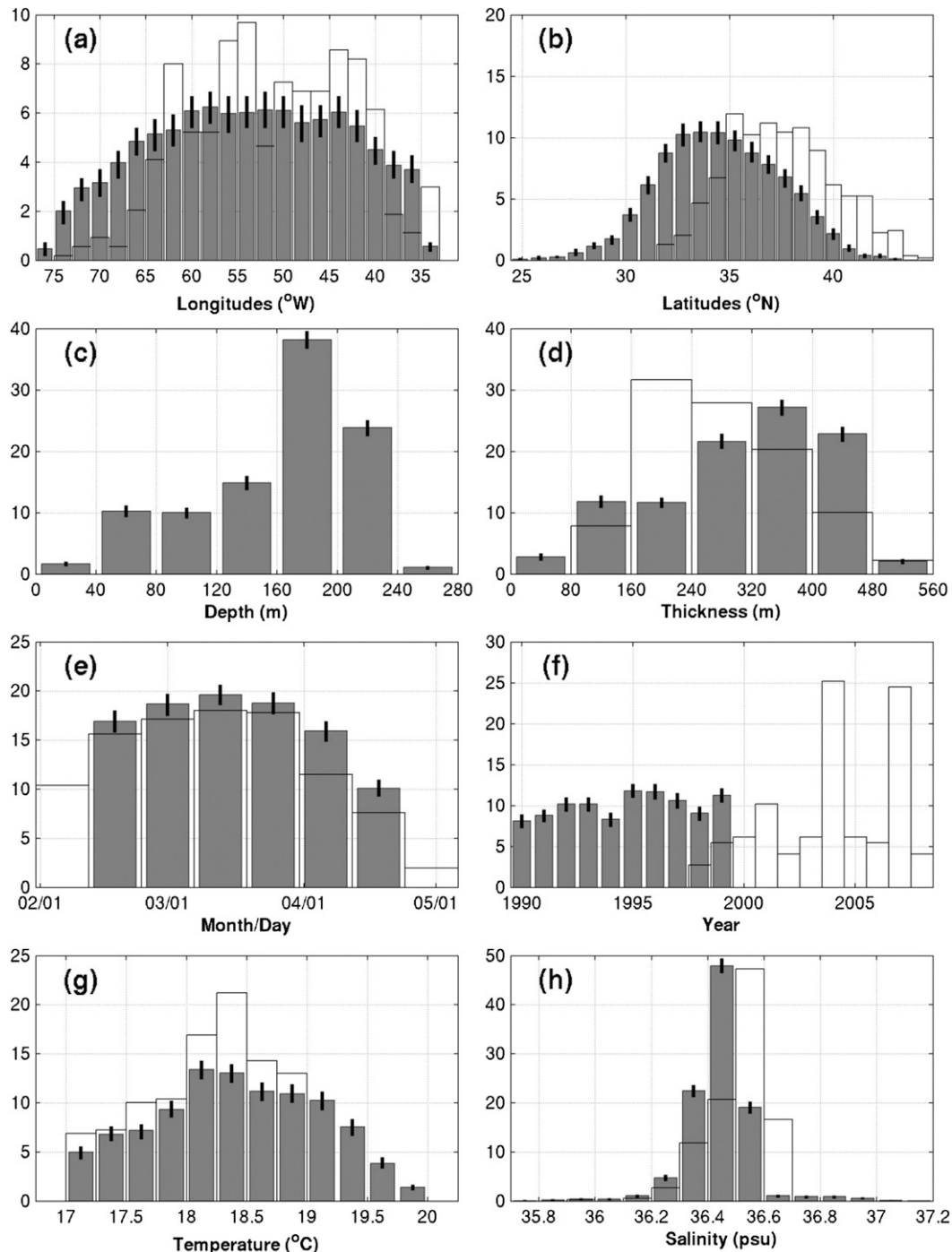
FIG. 4. Histograms of FLAME particles at the time of deployment (near the middle of the outcropped the EDW column) (gray bars) and the observed EDW outcropping from the profiling floats (white bars) for (a) longitude, (b) latitude, (c) depth of the particles, (d) thickness of the outcropped EDW column (in which the particles are deployed), (e) dates (regardless of year), (f) year, (g) potential temperature, and (h) salinity. Note that each histogram is normalized by the total number of data (49 753 for particles and 538 for the observations), and therefore the unit of the y axes is percentage of total. The error bars indicate the 25–75 percentile range calculated based on 5000 randomly selected groups of FLAME particles, where the group size matches the number of profiling float observations (538).
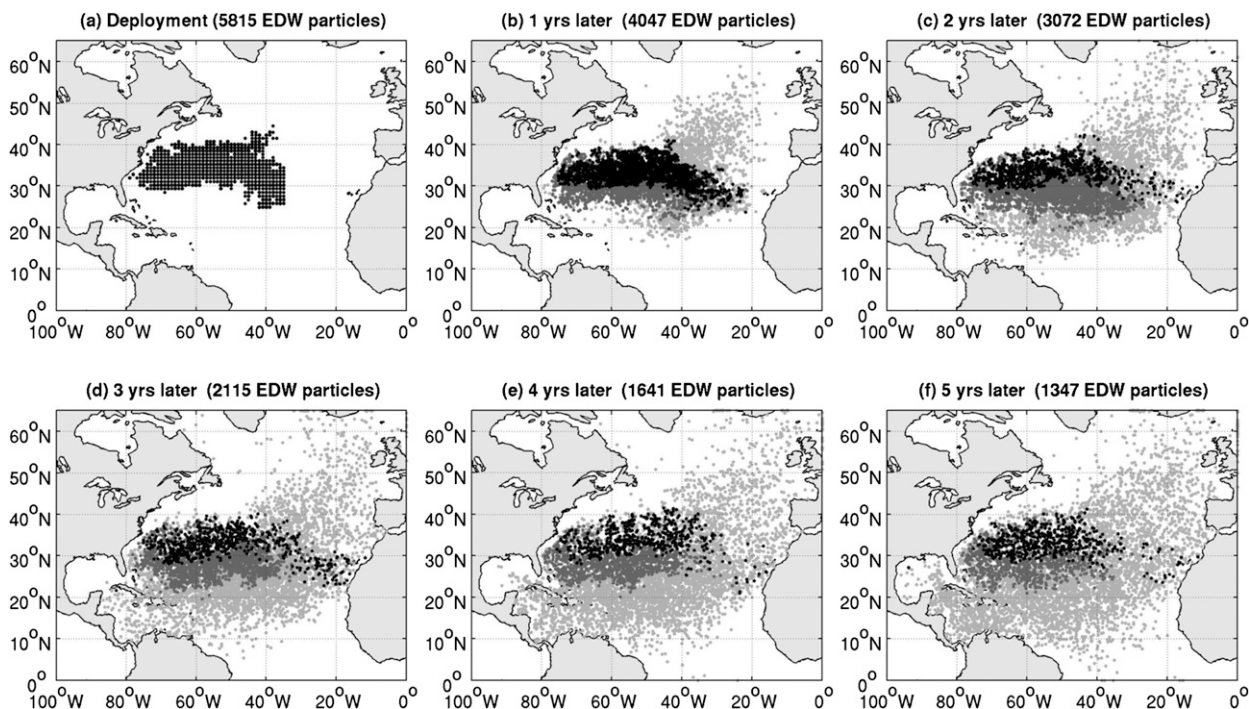
FIG. 5. Positions of ~5700 particles at six different trajectory lengths since deployment in February–April 1996. Black dots indicate particles within the outcropped EDW at the time of each snapshot, dark gray dots are for those remaining within the nonoutcropping EDW, and the light gray denote those particles that no longer satisfy the definition of the EDW. Note that lighter dots may exist underneath darker ones.

quickly advect to the northeast, they largely remain south of the North Atlantic Current within the subtropical gyre, consistent with the more detailed analysis of float trajectories and intergyre exchange by Burkholder and Lozier (2011). While the particles over time gradually cover a larger area to the south of the North Atlantic Current, the region where EDW is found (i.e., gray and black dots) remains to the north of ~20°N and west of ~35°W.

Most relevant to the focus of this paper is the rather stable outcropping extent, indicated by black dots. EDW outcropping is generally bounded by ~30°N and ~35°W, except for the eastward extension toward the Madeira Mode Water, especially after 1–3 yr (Figs. 5b–d). The rather stable extent of the outcropping region implies that the reoutcropping time scale will primarily be determined by how long particles remain in this outcropping region or how long it takes them to come back to this outcropping region.

To illuminate the concentration of particles found in the EDW at 1-yr intervals, a two-dimensional histogram of all particles is shown in Fig. 6. The sum of particles over the domain initially equals those deployed (100%) and then gradually decreases as more particles become non-EDW. Overall, the histogram indicates that the region of highest particle concentration slowly moves

southward, crossing the southern boundary of the outcropping region (marked by white lines in Figs. 6b–f), and then westward, moving anticyclonically with time. In particular, Fig. 6b suggests that the majority of particles remain within the outcropping region after 1 yr. While no apparent sense of the mean circulation can be easily seen from the overall distribution shown in Fig. 5, the mean position of the particles moves in the direction of the mean anticyclonic gyre circulation, as quantitatively shown in Fig. 6f. Note that the mean position is calculated for only the particles in EDW.

Quantitatively, 30% of particles are found in non-EDW waters 9 months after the deployment, and only 25% are found within EDW after 5 yr, corresponding to an e-folding time scale of 3–3.5 yr (gray curve in Fig. 7). Note that Fig. 7 is not restricted to the particles that remain continuously within EDW since their deployments (cf. Gary et al. 2014). A small number of them, having lost their EDW characteristics, acquire them again, as can be seen from the small increase in the number of EDW particles after about 1 yr (Fig. 7). Some of the particles are found in outcropping EDW in the following winters; that is, they reoutcrop as EDW, as indicated by the gray shading in Fig. 7. As the particles escape from the outcropping region, the ratio between the number of particles in outcropped EDW (shading in
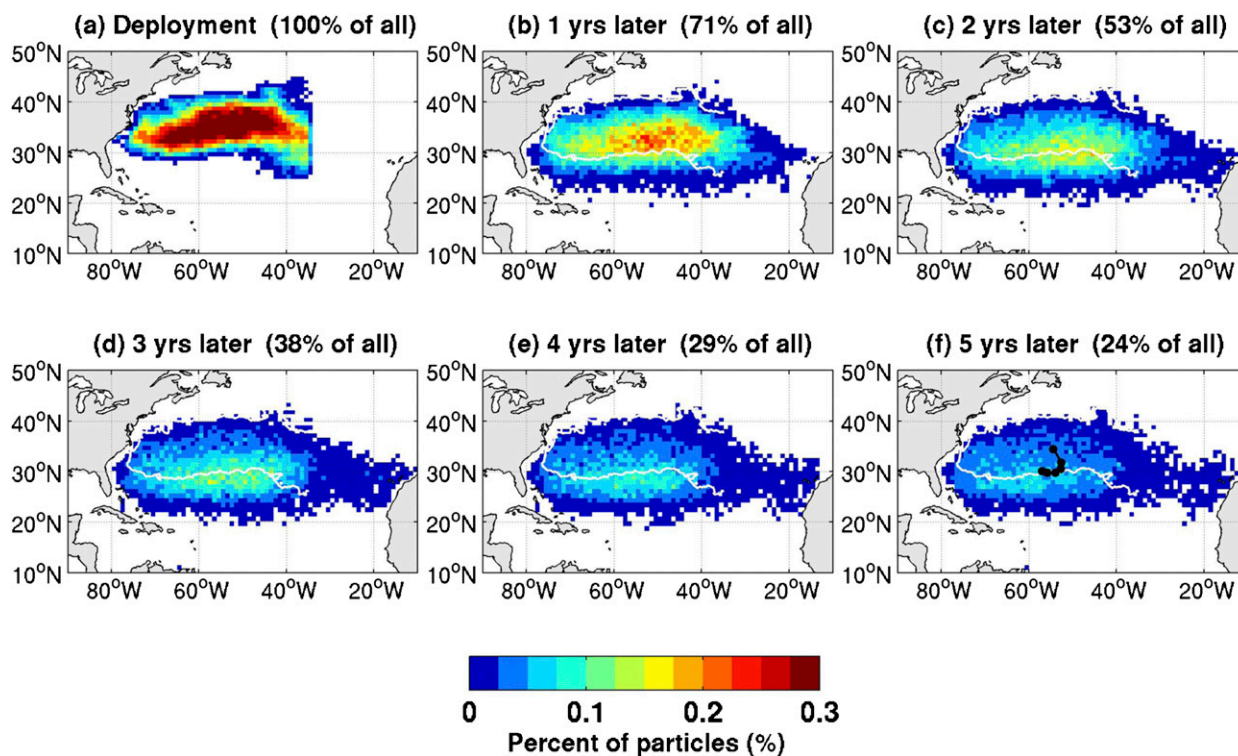
FIG. 6. Census of all particles found within EDW at yearly intervals. Each panel is for a different time since deployment. Color indicates the percent of particles in each 1° × 1° bin out of all 49 753 deployed particles. Its integral over the entire domain is reported in the title of each panel. In (b)–(f) the white lines denote the 10% outcropping region from Fig. 2. The black dots in (f) indicate the mean position of the particles in EDW at each of the six yearly snapshots, which slowly move anticyclonically.

Fig. 7) to the total number in EDW (gray curve in Fig. 7) decreases each winter: 55%, 42%, and 33% after 1, 2, and 3 yr, respectively, indicating that fewer and fewer particles stay within or near the outcropping region over time.

b. Reoutcropping of the EDW

We next examine the time elapsed between the deployment and the first reoutcropping. A histogram of the time to reoutcropping as EDW (for the first time since deployment) shows that 66% of all particles reoutcrop after 1 yr. This fraction drops to below 5% for the out years without any noticeable secondary peak (Fig. 8). We note that while it is possible for particles to spend some portion of their time as non-EDW before reoutcropping, they are nonetheless included in this count. When only particles that continuously remain in EDW until reoutcropping are counted, 19% of all particles reoutcrop as EDW after 1 yr, and that fraction becomes less than 1% for the out years; 80% become non-EDW at least temporarily before reoutcropping. [Please see Gary et al. (2014) for an explanation of how particles exit from and reenter EDW on relatively short time scales.] Also note that each particle is counted only

once in Fig. 8 for the first reoutcropping since deployment, while the particles are repeatedly counted at each time step in Fig. 7, which is a census at each given time. Therefore, neither the peak value nor integration of the gray shading in year 1 of Fig. 7 equals 66%.

The histogram of reoutcropping time (Fig. 8) is consistent with the slow dispersal previously discussed. The predominant peak for the reoutcropping at 1 yr indicates that 1 yr is not long enough for the majority of particles to escape from the EDW outcropping region, as illustrated with the 10 randomly chosen trajectories with 1-yr reoutcropping (Fig. 9a). However, particles deployed close to the boundary of the outcropping region have a greater chance to advect out of the outcropping region before the following winter. Indeed, the gray shading in Figs. 9b–c shows that the particles that take 3 and 5 yr to reoutcrop are more likely deployed near the southern boundary of the outcropping region. Furthermore, particles that take 3 yr to reoutcrop are deployed mostly near the southwestern corner of the EDW outcropping region (to the west of 60°W), while those that take 5 yr are mostly deployed to the east of 60°W. Note that particles remaining in the outcropping region are not necessarily outcropping nor in EDW (dashed curve vs
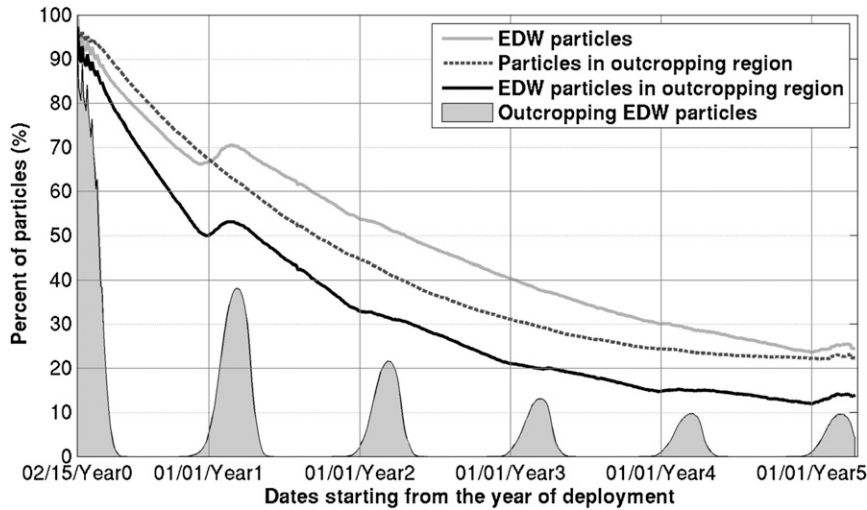
FIG. 7. Percentage of particles as a function of time since deployment. Gray curve is for the particles found within EDW anywhere in the domain. Dashed curve is for all the particles found within the 10% outcropping region from Fig. 2, including both EDW and non-EDW particles. Solid black curve is for the EDW particles found within the 10% outcropping region from Fig. 2. Shading is for the outcropping EDW particles within the 10% outcropping region from Fig. 2. All percentages are relative to the initial number of particles (49 753). All particles that meet the stated criteria are counted at each time step, meaning particles can be counted more than once.

solid black curve in Fig. 7). However, the relative proportion of particles in the outcropping region that actually outcrop in EDW is fairly constant, as can be seen from the dashed curve and shading in Fig. 7.

The randomly chosen trajectories reveal that particles that reoutcrop in 1 yr are characterized by eddy-like motions (Fig. 9a). On the contrary, particles that take 3 yr to outcrop, while also characterized by eddy-like motions, clearly trace the mean anticyclonic gyre circulation (Fig. 9b). These particles exit the outcropping region in less than a year, yet come back to the region, generally via the Gulf Stream, in about 3 yr. The particles that take 5 yr to reoutcrop have even longer anticyclonic pathways, consistent with the mean streamfunction for the isopycnal layer bounded by $\sigma_\theta = 26.1$ and $26.5 \, \mathrm{kg \, m^{-3}}$ (Fig. 10), especially those deployed in the southeastern part of the outcropping region. These take longer to come back to the outcropping region (Fig. 9c).

To gain further insight into the respective roles that mean and time-dependent circulation play in EDW outcropping, trajectories of particles are recalculated as before except instead of using time-dependent variables the climatological-mean monthly temperatures are used for the EDW definition and particle deployment and the climatological-mean monthly velocities are used for the trajectory calculations. A two-dimensional histogram of the resulting particle distribution (Fig. 11) reveals the mean advective path more clearly than the histogram derived from the use of the time-dependent velocity

field (Fig. 6). As expected, there is less spread in the pathways in the mean velocity case; however, the advection of the mean position (shown as the black dots in Fig. 11f) is comparable to that from the full velocity case
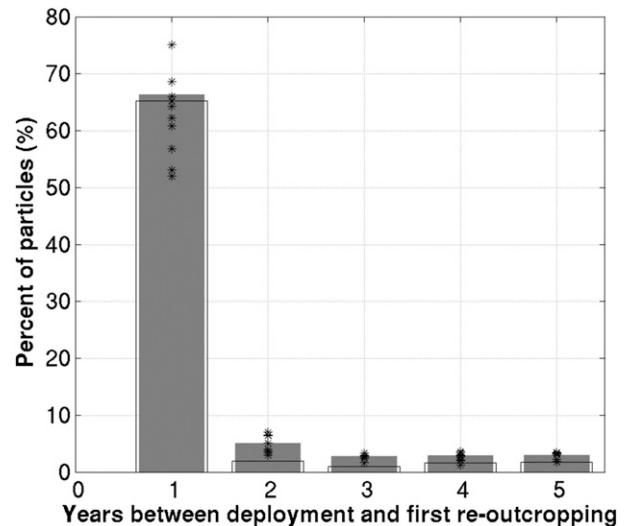

FIG. 8. Histogram of the time for a particle to reoutcrop as EDW for the first time since deployment. (Note that each particle is counted only once.) The gray bars are from the particles of which trajectories are calculated using full 3-daily velocity and temperature fields from all 10 winter deployments, while the stars are from the corresponding calculations for each winter's deployment separately. The white bars are from those trajectories calculated using only the climatological monthly-mean velocity and temperature.
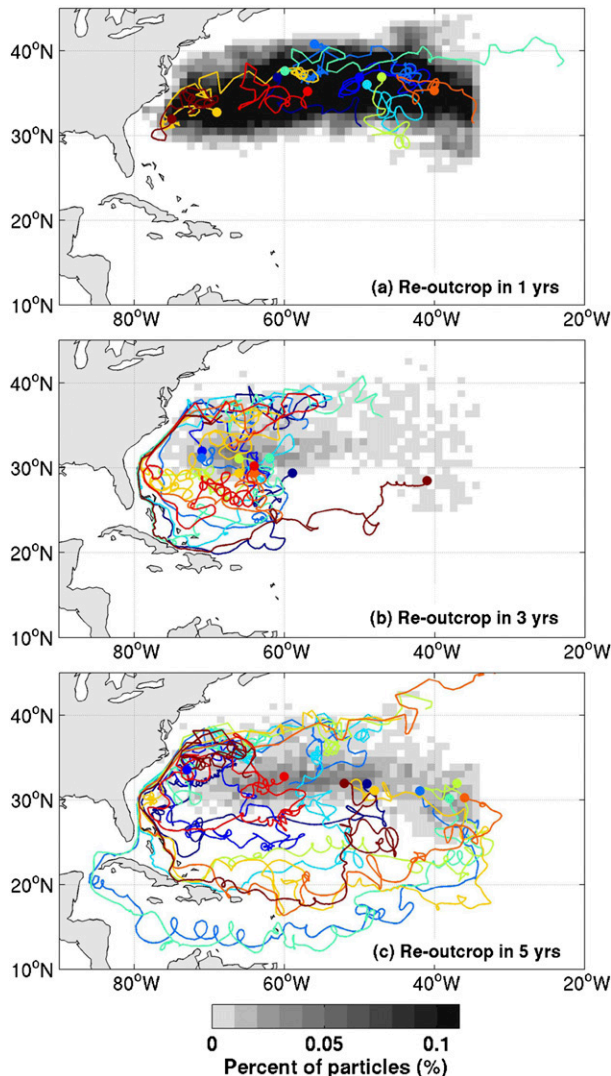
FIG. 9. The 10 randomly selected trajectories for each re-outcropping time. Each deployment position is indicated with a filled circle, and the other end of each curve is the reoutcropped position. The gray shadings are the two-dimensional histograms of the original deployment positions for the particles with each reoutcropping time. The histogram is calculated as the percentage of the total particles deployed (49 753).
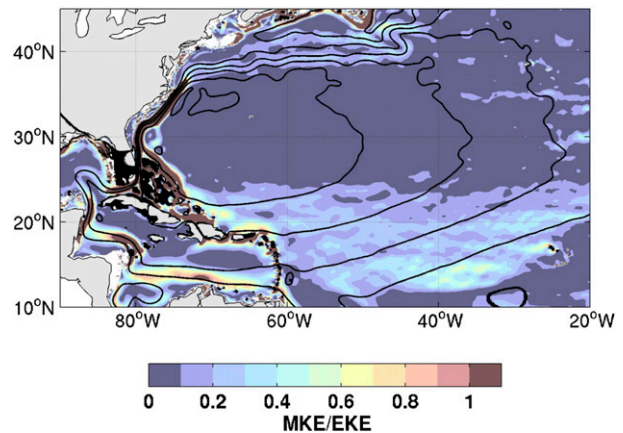

FIG. 10. Time-mean FLAME streamfunction (black contours) and the ratio between the MKE and EKE (color shading) for the isopycnal layer bounded by $\sigma_\theta = 26.1$ and $26.5\,\mathrm{kg\,m^{-3}}$. Contour interval for the streamfunction is $2 \times 10^4\,\mathrm{m^2\,s^{-1}}$.

region. Since the horizontal eddy diffusivity around the EDW outcropping region is approximately $10^4\,\mathrm{m^2\,s^{-1}}$ (Lumpkin et al. 2002; McClean et al. 2002; Fratantoni et al. 2013) and the outcropping area is $\sim 3.5 \times 10^{12}\,\mathrm{m^2}$, the eddy diffusive time scale for a particle to escape the outcropping region is $\sim 10\,\mathrm{yr}$, implying that the eddy field is not strong enough to be a dominant factor in the advection of particles out of the outcropping region. Local values of eddy kinetic energy (EKE) are an order of magnitude greater than mean kinetic energy (MKE) over most of the outcropping region (Fig. 10), consistent with the eddy-like trajectories in Fig. 9a. Though these eddy-like motions contribute to the vigorous local advection, the reoutcropping time scale is controlled by the mean flow. Note that the time-dependent circulation (as opposed to the mean circulation) results from not only the presence of mesoscale eddies but also from other transient circulations, for example, Gulf Stream meandering and the interannual variability of the large-scale circulation.

5. Summary and discussion

EDW outcropping is analyzed with Lagrangian trajectories of particles from the eddy-resolving FLAME simulation. In each winter from 1990 to 1999, particles were deployed in the center of outcropped EDW columns. Subsequently, the trajectories of these particles were calculated for the following 5 yr. Compared to profiling float observations from 1998 to 2008 and WOCE hydrographic sections, the spatial and temporal distributions of EDW, including the winter outcropping, are realistically reproduced in the FLAME simulation.

Following the deployment, the particles slowly spread from the outcropped region into the nonoutcropping

(Fig. 6f). Furthermore, almost identical percentages of particles reoutcrop in 1 yr in the mean velocity case (white bars in the Fig. 8) compared to the time-dependent velocity case. However, when the full time-dependent velocity case is calculated separately for each winter's deployment, the amplitudes of the 1-yr reoutcropping vary by about ±10%, reflecting interannual variability in both outcropping and the circulation.

This result suggests that the dominant 1-yr reoutcropping is primarily determined by the mean circulation. Essentially, the reoutcropping time scale is primarily set by how long the particles can stay within the outcropping
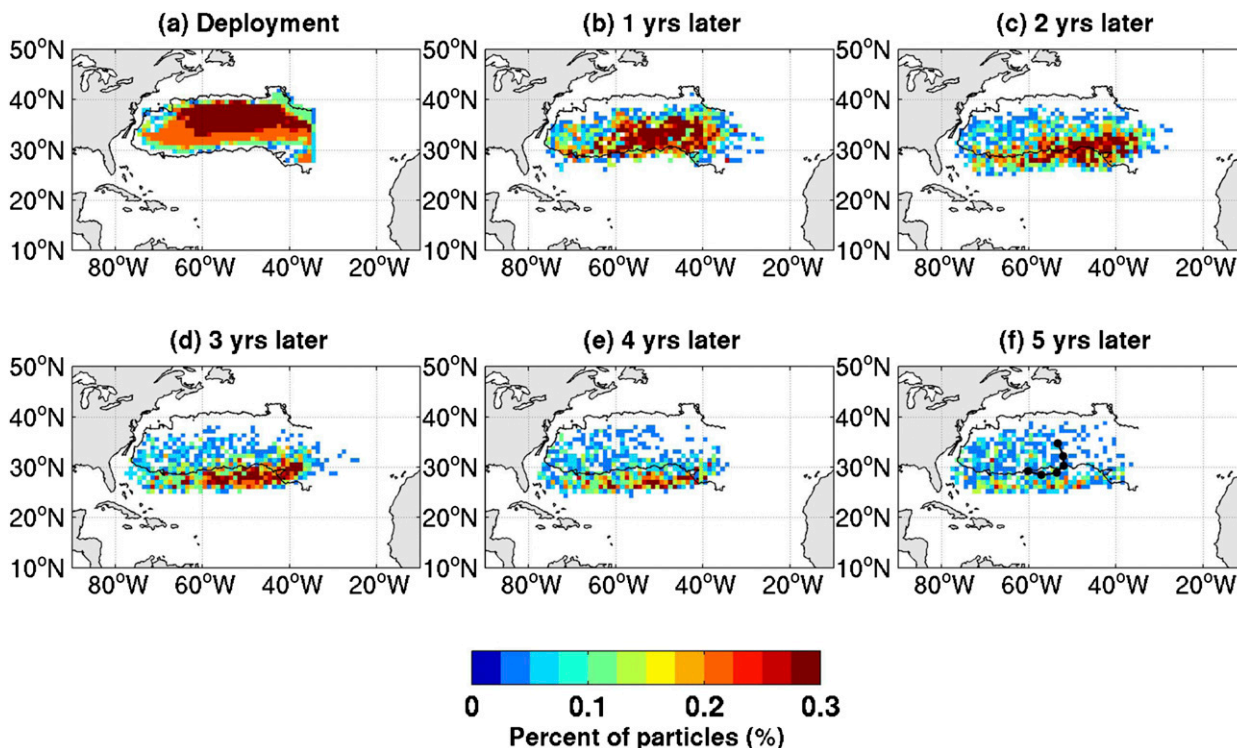
FIG. 11. As in Fig. 6, but the Lagrangian trajectories are calculated using the climatological monthly-mean velocity fields. Black lines denote the 10% outcropping region from Fig. 2.

EDW region south of 30°N and eventually to the non-EDW region in the subtropical gyre. While the mean position of all particles in EDW traces the anticyclonic subtropical gyre circulation, individual trajectories are heavily impacted by mesoscale features. Approximately 30% of the particles are found to be non-EDW 1 yr after the deployment, and after 5 yr, only 25% of the particles are found within EDW. The majority of EDW to non-EDW transitions can be attributed to increasing stratification that destroys the thermostad (Gary et al. 2014).

In the winter immediately following deployment, up to 66% of the deployed particles reoutcrop as EDW (i.e., they are found in the outcropping EDW column). The particles that take 2 to 5 yr before reoutcropping compose less than 14% of the total (with less than 5% for each yr), consistent with an e-folding time scale of 1.5–2 yr for particles found in the EDW outcropping region (black curve in Fig. 7). Fratantoni et al. (2013) reported a similar result from a study of quasi-Lagrangian CLIMODE bobber float observations, although from a limited sample number. In that study, 37 out of 55 observed EDW outcropping events were followed by reoutcropping in the next winter.

There is an apparent discrepancy between the 1-yr reoutcropping time and the ~3–4-yr turnover time for EDW estimated from previous studies (Jenkins 1982; Kwon and Riser 2004), but the two time scales measure two different aspects of the water mass history (see also Gary et al. 2014). The difference implies that EDW age (or the time since the last outcropping) has a skewed probability distribution, with the mode at a young age and a very long tail toward older ages. Indeed, Douglass et al. (2013) found such a skewed distribution of EDW ideal age in an eddy-resolving ocean model simulation, where there was a long tail out to 15 yr. The oldest EDW was concentrated in the southwestern corner of the EDW pool in their study. Gary et al. (2014) also showed that the Lagrangian age of EDW particles increases rapidly to the south of the outcropping region, with the oldest ages found in the southwestern corner of the EDW region.

Because EDW lies within the anticyclonic subtropical gyre, the role of the mean geostrophic circulation for the subduction and circulation of EDW has often been emphasized (e.g., Kwon and Riser 2004; Kelly and Dong 2013). However, recent CLIMODE observations clearly suggest a significant role for eddies in EDW formation (Davis et al. 2013; Joyce et al. 2009) and circulation (Fratantoni et al. 2013). Consistent with those studies, trajectories from the CLIMODE bobber floats and from
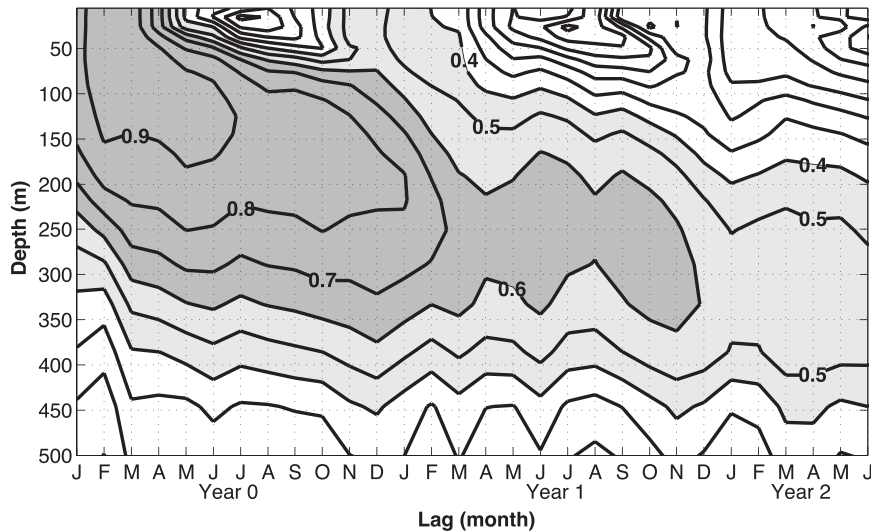
FIG. 12. Lagged correlations between monthly temperature time series at each depth and the time series of temperature averaged over the upper 100 m for February–March. Both time series use monthly temperatures averaged over the 10% outcropping region shown in Fig. 2. Correlations greater than 0.6 (0.4) are shaded with dark (light) gray.

the FLAME particles are indeed often dominated by strong eddylike motions, even though their average pathways reflect the large-scale circulation (see the mean streamfunction in Fig. 10).

The reoutcropping time scale is primarily set by how long the particles can stay within the outcropping region. Comparisons between trajectories calculated from the mean velocity and those calculated from the time-dependent velocity suggest that the dominant, 1-yr reoutcropping is primarily determined by the mean circulation, while the year-to-year variability accounts for changes in the 1-yr reoutcropping by about ±10%. The time for remaining in the outcropping region is also a function of the spatial extent of the outcropping region, which depends upon the EDW definition. For example, if a narrower temperature range of 17°–19°C is used, the percentage of particles with a 1-yr reoutcropping decreases by ~3%; by reducing the vertical temperature gradient to 0.006°C m^{-1}, the percentage decreases by ~13%. However, the dominance of the 1-yr reoutcropping time is robust; that is, it is relatively insensitive to the EDW definition.

As mentioned above, the signature of past air–sea interaction stored in EDW could influence future air–sea interaction through reoutcroppings and thereby contribute to low-frequency climate variability. The concentration of reoutcropping in 1 yr suggests that EDW provides an effective bridge from 1 yr to the next but that it does not bridge multiple years. When the EDW outcropping region is considered as a whole, the year-to-year reoutcropping is analogous to the

one-dimensional reemergence mechanism of winter sea surface temperature (Alexander and Deser 1995; Timlin et al. 2002). To demonstrate the effect of the reemergence, February–March temperature anomalies in the upper 100 m in the outcropping region are correlated with subsurface temperature anomalies at different lags (Fig. 12). The upper 100-m temperature anomalies in February–March exhibit a correlation up to $r = 0.5$ with the surface temperature anomalies in the following winter, but the correlation drops rapidly for subsequent winters. On the other hand, the correlation between 200 and 400 m stays above $r = 0.5$ for up to 2.5 yr. While the persistence of temperature anomalies along individual trajectories is limited to ~3 months because of mixing (Gary et al. 2014), average anomalies of EDW taken as a whole are found to persist for multiple years. This result, combined with previous studies that demonstrated the dominant role of geostrophic heat flux convergence compared to the local air–sea heat flux in the upper-ocean heat budget for interannual time scale in this region (Dong and Kelly 2004; Dong et al. 2007; Buckley et al. 2014), suggests a potential role of ocean memory associated with EDW in low-frequency climate variability.

This study focuses on EDW pathways following EDW formation. An equally important and complementary study would focus on the origin of the waters that form EDW. Our results suggest that ~65% of the outcropping EDW columns each winter have their origin as EDW from the preceding year. When the previous 5 yr are considered (by summing all 5 yr in Fig. 8), 80% of the

outcropping EDW columns can be traced back to the earlier EDW outcropping columns. Therefore, 20% or more of the newly produced EDW each year needs to originate from a non-EDW region. Joyce et al. (2013), based on a salinity budget of hydrographic observations, suggested that the cold and fresh subpolar water in the northern recirculation is a necessary ingredient for newly produced EDW. Though our trajectory study was not designed to address the origin of the water parcels constituting the newly produced EDW, our results are not inconsistent with this suggestion. Backward trajectory calculations starting from the winter EDW outcropping, as used in the study of pathways of the Labrador Sea Water (Bower et al. 2009) and the North Atlantic Subpolar Mode Water (de Boisséson et al. 2012), would be needed to make this linkage more explicit.

REFERENCES

Alexander, M. A., and C. Deser, 1995: A mechanism for the recurrence of wintertime midlatitude SST anomalies. *J. Phys. Oceanogr.,* **25,** 122–137, doi:10.1175/1520-0485(1995)025<0122:AMFTRO>2.0.CO;2.

Alfultis, M., and P. Cornillon, 2001: Annual and interannual changes in the North Atlantic subtropical mode water layer properties. *J. Phys. Oceanogr.,* **31,** 2066–2086, doi:10.1175/1520-0485(2001)031<2066:AAICIT>2.0.CO;2.

Bates, N. R., A. C. Pequignet, R. J. Johnson, and N. Gruber, 2002: A short-term sink for atmospheric CO_2 in subtropical mode water of the North Atlantic Ocean. *Nature,* **420,** 489–493, doi:10.1038/nature01253.

Beckmann, A., and R. Döscher, 1997: A method for improved representation of dense water spreading over topography in geopotential-coordinate models. *J. Phys. Oceanogr.,* **27,** 581–591, doi:10.1175/1520-0485(1997)027<0581:AMFIRO>2.0.CO;2.

Biastoch, A., C. W. Böning, J. Getzlaff, J. M. Molines, and G. Madec, 2008: Causes of interannual–decadal variability in the meridional overturning circulation of the midlatitude North Atlantic Ocean. *J. Climate,* **21,** 6599–6615, doi:10.1175/2008JCLI2404.1.

Billheimer, S., and L. D. Talley, 2013: Near cessation of Eighteen Degree Water renewal in the western North Atlantic in the warm winter of 2011–2012. *J. Geophys. Res. Oceans,* **118,** 6838–6853, doi:10.1002/2013JC009024.

Böning, C. W., M. Scheinert, J. Dengg, A. Biastoch, and A. Funk, 2006: Decadal variability of subpolar gyre transport and its

reverberation in the North Atlantic overturning. *Geophys. Res. Lett.,* **33,** L21S01, doi:10.1029/2006GL026906.

Bower, A. S., M. S. Lozier, S. F. Gary, and C. W. Böning, 2009: Interior pathways of the North Atlantic meridional overturning circulation. *Nature,* **459,** 243–247, doi:10.1038/nature07979.

Boyer, T. P., and S. Levitus, 1997: Objective analyses of temperature and salinity for the World Ocean on a 1/4° grid. NOAA Atlas NESDIS 11, 83 pp.

Buckley, M. W., R. M. Ponte, G. Forget, and P. Heimbach, 2014: Low-frequency SST and upper-ocean heat content variability in the North Atlantic. *J. Climate,* **27,** 4996–5018, doi:10.1175/JCLI-D-13-00316.1.

Burkholder, K. C., and M. S. Lozier, 2011: Subtropical to subpolar pathways in the North Atlantic: Deductions from Lagrangian trajectories. *J. Geophys. Res.,* **116,** C07017, doi:10.1029/2010JC006697.

Cayan, D. R., 1992: Latent and sensible heat flux anomalies over the northern oceans: The connection to monthly atmospheric circulation. *J. Climate,* **5,** 354–369, doi:10.1175/1520-0442(1992)005<0354:LASHFA>2.0.CO;2.

Cummins, P. F., G. Holloway, and A. E. Gargett, 1990: Sensitivity of the GFDL ocean general circulation model to a parameterization of vertical diffusion. *J. Phys. Oceanogr.,* **20,** 817–830, doi:10.1175/1520-0485(1990)020<0817:SOTGOG>2.0.CO;2.

Czeschel, L., 2004: The role of eddies for the deep water formation in the Labrador Sea. Ph.D. thesis, Christian-Albrechts-Universität, 101 pp.

Davis, X. J., F. Straneo, Y.-O. Kwon, K. A. Kelly, and J. M. Toole, 2013: Evolution and formation of North Atlantic Eighteen Degree Water in the Sargasso Sea from moored data. *Deep-Sea Res. II,* **91,** 11–24, doi:10.1016/j.dsr2.2013.02.024.

de Boisséson, E., V. Thierry, H. Mercier, G. Caniaux, and D. Desbruyères, 2012: Origin, formation and variability of the Subpolar Mode Water located over the Reykjanes Ridge. *J. Geophys. Res.,* **117,** C12005, doi:10.1029/2011JC007519.

Deremble, B., and W. K. Dewar, 2013: Volume and potential vorticity budgets of Eighteen Degree Water. *J. Phys. Oceanogr.,* **43,** 2309–2321, doi:10.1175/JPO-D-13-052.1.

——, N. Wienders, and W. K. Dewar, 2014: Potential vorticity budgets in the North Atlantic Ocean. *J. Phys. Oceanogr.,* **44,** 164–178, doi:10.1175/JPO-D-13-087.1.

Dickson, R., J. Lazier, J. Meincke, P. Rhines, and J. Swift, 1996: Long-term coordinated changes in the convective activity of the North Atlantic. *Prog. Oceanogr.,* **38,** 241–295, doi:10.1016/S0079-6611(97)00002-5.

Dong, S., and K. A. Kelly, 2004: Heat budget in the Gulf Stream region: The importance of heat storage and advection. *J. Phys. Oceanogr.,* **34,** 1214–1231, doi:10.1175/1520-0485(2004)034,1214:HBITGS.2.0.CO;2.

——, S. L. Hautala, and K. A. Kelly, 2007: Interannual variations in upper-ocean heat content and heat transport convergence in the western North Atlantic. *J. Phys. Oceanogr.,* **37,** 2682–2697, doi:10.1175/2007JPO3645.1.

Douglass, E. M., Y.-O. Kwon, and S. R. Jayne, 2013: A comparison of Subtropical Mode Waters in a climatologically-forced model. *Deep-Sea Res. II,* **91,** 139–151, doi:10.1016/j.dsr2.2013.02.023.

Forget, G., G. Maze, M. Buckley, and J. Marshall, 2011: Estimated seasonal cycle of North Atlantic Eighteen Degree water volume. *J. Phys. Oceanogr.,* **41,** 269–286, doi:10.1175/2010JPO4257.1.

Fratantoni, D. M., Y.-O. Kwon, and B. A. Hodges, 2013: Direct observation of Subtropical Mode Water circulation in the western North Atlantic Ocean. *Deep-Sea Res. II,* **91,** 35–56, doi:10.1016/j.dsr2.2013.02.027.

Gary, S. F., M. S. Lozier, C. Böning, and A. Biastoch, 2011: Deciphering the pathways for the deep limb of the meridional overturning circulation. *Deep-Sea Res. II,* **58,** 1781–1797, doi:10.1016/j.dsr2.2010.10.059.

——, ——, Y.-O. Kwon, and J.-J. Park, 2014: The fate of North Atlantic Subtropical Mode Water in the FLAME model. *J. Phys. Oceanogr.,* **44,** 1354–1371, doi:10.1175/JPO-D-13-0202.1.

Hanawa, K., and L. Talley, 2001: Mode waters. *Ocean Circulation and Climate,* G. Siedler, J. Church, and J. Gould, Eds., International Geophysics Series, Vol. 77, Academic Press, 373–386.

Jenkins, W. J., 1982: On the climate of a subtropical ocean gyre: Decadal time scale variations in water mass renewal in the Sargasso Sea. *J. Mar. Res.,* **40,** 265–290.

Joyce, T. M., 2012: New perspectives on Eighteen-Degree Water formation in the North Atlantic. *J. Oceanogr.,* **68,** 45–52, doi:10.1007/s10872-011-0029-0.

——, R. S. Pickart, and R. C. Millard, 1999: Long-term hydrographic changes at 52 and 66°W in the North Atlantic Subtropical Gyre & Caribbean. *Deep-Sea Res. II,* **46,** 245–278, doi:10.1016/S0967-0645(98)00102-7.

——, L. Thomas, and F. Bahr, 2009: Wintertime observations of Subtropical Mode Water formation within the Gulf Stream. *Geophys. Res. Lett.,* **36,** L02607, doi:10.1029/2008GL035918.

——, ——, W. K. Dewar, and J. B. Girton, 2013: Eighteen Degree Water formation within the Gulf Stream during CLIMODE. *Deep-Sea Res. II,* **91,** 1–10, doi:10.1016/j.dsr2.2013.02.019.

Kalnay, E. M., and Coauthors, 1996: The NCEP/NCAR 40-Year Reanalysis Project. *Bull. Amer. Meteor. Soc.,* **77,** 437–471, doi:10.1175/1520-0477(1996)077<0437:TNYRP>2.0.CO;2.

Kelly, K. A., and S. Dong, 2013: The contributions of atmosphere and ocean to North Atlantic Subtropical Mode Water volume anomalies. *Deep-Sea Res. II,* **91,** 111–127, doi:10.1016/j.dsr2.2013.02.020.

Kraus, E. B., and J. S. Turner, 1967: A one-dimensional model of the seasonal thermocline. II. The general theory and its consequences. *Tellus,* **19,** 98–106, doi:10.1111/j.2153-3490.1967.tb01462.x.

Kwon, Y.-O., 2003: Observation of general circulation and water mass variability in the North Atlantic subtropical mode water region. Ph.D. thesis, University of Washington, 161 pp.

——, and S. C. Riser, 2004: North Atlantic Subtropical Mode Water: A history of ocean-atmosphere interaction 1961–2000. *Geophys. Res. Lett.,* **31,** L19307, doi:10.1029/2004GL021116.

——, and ——, 2005: The general circulation of the western subtropical North Atlantic observed using profiling floats. *J. Geophys. Res.,* **110,** C10012, doi:10.1029/2005JC002909.

Levitus, S., and T. P. Boyer, 1994: *Temperature.* Vol. 4, *World Ocean Atlas 1994,* NOAA Atlas NESDIS 4, 117 pp.

——, R. Burgett, and T. P. Boyer, 1994: *Salinity.* Vol. 3, *World Ocean Atlas 1994,* NOAA Atlas NESDIS 3, 99 pp.

Lumpkin, R., A.-M. Treguier, and K. Speer, 2002: Lagrangian eddy scales in the Northern Atlantic Ocean. *J. Phys. Oceanogr.,* **32,** 2425–2440, doi:10.1175/1520-0485-32.9.2425.

Marshall, J., D. Jamous, and J. Nilsson, 1999: Reconciling thermodynamic and dynamic methods of computation of water-mass transformation rates. *Deep-Sea Res.,* **46,** 545–572, doi:10.1016/S0967-0637(98)00082-X.

——, and Coauthors, 2009: Observing the cycle of convection and restratification over the Gulf Stream system and the subtropical gyre of the North Atlantic Ocean: Preliminary results from the CLIMODE field campaign. *Bull. Amer. Meteor. Soc.,* **90,** 1337–1350, doi:10.1175/2009BAMS2706.1.

Maze, G., and J. Marshall, 2011: Diagnosing the observed seasonal cycle of Atlantic subtropical mode water using potential vorticity and its attendant theorems. *J. Phys. Oceanogr.,* **41,** 1986–1999, doi:10.1175/2011JPO4576.1.

——, G. Forget, M. Buckley, J. Marshall, and I. Cerovečki, 2009: Using Transformation and formation maps to study the role of air–sea heat fluxes in North Atlantic Eighteen Degree Water formation. *J. Phys. Oceanogr.,* **39,** 1818–1835, doi:10.1175/2009JPO3985.1.

——, J. Deshayes, J. Marshall, A.-M. Tréguier, A. Chronis, and L. Vollmer, 2013: Surface vertical PV fluxes and subtropical mode water formation in an eddy-resolving numerical simulation. *Deep-Sea Res. II,* **91,** 128–138, doi:10.1016/j.dsr2.2013.02.026.

McClean, J. L., P.-M. Poulain, J. W. Pelton, and M. E. Maltrud, 2002: Eulerian and Lagrangian statistics from surface drifters and a high-resolution POP simulation in the North Atlantic. *J. Phys. Oceanogr.,* **32,** 2472–2491, doi:10.1175/1520-0485-32.9.2472.

Olsina, O., N. Wienders, and W. K. Dewar, 2013: An estimate of the climatology and variability of Eighteen Degree Water potential vorticity forcing. *Deep-Sea Res. II,* **91,** 84–95, doi:10.1016/j.dsr2.2013.02.018.

Pacanowski, R. C., 1996: MOM 2 version 2.0 (beta): Documentation, user's guide, and reference manual. GFDL Ocean Tech. Rep. 3.2, 350 pp.

Palter, J. B., M. S. Lozier, and R. T. Barber, 2005: The effect of advection on the nutrient reservoir in the North Atlantic subtropical gyre. *Nature,* **437,** 687–692, doi:10.1038/nature03969.

Siedler, G., A. Kuhl, and W. Zenk, 1987: The Madeira Mode Water. *J. Phys. Oceanogr.,* **17,** 1561–1570, doi:10.1175/1520-0485(1987)017<1561:TMMW>2.0.CO;2.

Speer, K., and E. Tziperman, 1992: Rates of water mass formation in the North Atlantic Ocean. *J. Phys. Oceanogr.,* **22,** 93–104, doi:10.1175/1520-0485(1992)022<0093:ROWMFI>2.0.CO;2.

——, and G. Forget, 2013: Global distribution and formation of mode waters. *Ocean Circulation and Climate: A 21st Century Perspective,* G. Siedler et al., Eds., International Geophysics Series, Vol. 103, Academic Press, 211–226.

Talley, L., 1996: North Atlantic circulation and variability reviewed for the CNLS conference. *Physica D,* **98,** 625–646, doi:10.1016/0167-2789(96)00123-6.

——, and M. Raymer, 1982: Eighteen Degree Water variability. *J. Mar. Res.,* **40,** 757–775.

Timlin, M. S., M. A. Alexander, and C. Deser, 2002: On the reemergence of North Atlantic SST anomalies. *J. Climate,* **15,** 2707–2712, doi:10.1175/1520-0442(2002)015<2707:OTRONA>2.0.CO;2.

Walin, G., 1982: On the relation between sea-surface heat flow and thermal circulation in the ocean. *Tellus,* **34,** 187–195, doi:10.1111/j.2153-3490.1982.tb01806.x.

Worthington, L. V., 1959: The 18°C water in the Sargasso Sea. *Deep-Sea Res.,* **5,** 297–305, doi:10.1016/0146-6313(58)90026-1.

——, 1972: Anticyclogenesis in the oceans as a result of outbreaks of continental polar air. *Studies in Physical Oceanography: A Tribute to Georg Wust on His 80th Birthday,* A. L. Gordon, Ed., Gordon & Breach, 169–178.

——, 1976: On *the North Atlantic Circulation.* Johns Hopkins Oceanographic Studies, Vol. 6, Johns Hopkins University Press, 110 pp.

Wyville-Thompson, C., 1877: *The Voyage of the Challenger. The Atlantic.* Vol. 1. Macmillan, 498 pp.